JJBS

Volume 19, Number 1,March 2026
ISSN 1995-6673
Pages 113 – 125
https://doi.org/10.54319/jjbs/190111

Jordan Journal of Biological Sciences

Green Valorization of Coconut Husk Waste: NaOH-Activated Carbon for Improved Ammonia Filtration in Recirculating Aquaculture of Common Carp (*Cyprinus carpio*)

Said Ali Akbar[1,*], Raudhatul Jannah[1], Cut Nuzlia[1], Muhammad Hasan[2]

[1]*Department of Aquaculture, Faculty of Marine and Fisheries, Universitas Syiah Kuala, Banda Aceh, 23111, Indonesia;* [2]*Department of Chemistry Education, Faculty of Teacher Training and Education, Universitas Syiah Kuala. Banda Aceh 23111, Aceh, Indonesia*

Received: June 13, 2025; Revised: August 4, 2025; Accepted: August 11, 2025

Abstract

This study evaluated the efficacy of coconut husk-derived NaOH-activated carbon in improving water quality and fish health in a recirculating aquaculture system (RAS) for *Cyprinus carpio*. Activated carbon was synthesized via carbonization at 300 °C followed by NaOH activation, resulting in enhanced adsorption properties: surface area increased from 323.12 to 654.43 m²/g, iodine number rose from 687.43 to 992.95 mg/g, and methylene blue adsorption reached 132.12 mg/g. A 28-day RAS experiment was conducted with five treatments (0, 5, 10, 15, and 20 g of activated carbon), evaluating ammonia levels, oxidative stress responses, hematological status, erythrocyte morphology, and survival rate. Ammonia levels significantly decreased ($p < 0.05$), with P5 achieving 0.0103 ± 0.0006 ppm on Day 20, below regulatory thresholds. Antioxidant enzymes improved significantly (SOD: 8.575 U/mL; CAT: 0.09125 U/mL), while lipid peroxidation (MDA: 1.3 µmol/L) was reduced ($p < 0.05$). Oxygen consumption increased in P5 (220 ± 4 mg O_2/kg/h), and hematological parameters improved (MCHC: 33.52 ± 0.24 g/dL; MCV: 362.50 ± 29.01 fL; RBC: $2.08 \pm 0.02 \times 10^6$/µL), while WBC decreased ($52.5 \pm 5.25 \times 10^3$/µL). Erythrocyte deformities were minimized, and survival increased from 67.5% (control) to 97.5% in P5 ($p < 0.05$). This study underscores the potential of coconut husk-based activated carbon as a cost-effective and sustainable adsorbent, enhancing aquaculture water quality and fish welfare in RAS applications.

Keywords: activated carbon; ammonia removal; recirculating aquaculture; oxidative stress; fish hematology

1. Introduction

Cyprinus carpio is widely favored in freshwater aquaculture due to its adaptability to a wide range of environmental conditions, its fast growth, and its high feed-to-biomass conversion efficiency, traits that make it especially suitable for intensive aquaculture systems (Karatas et al., 2025). This species serves as a vital economic asset, contributing substantially to the profitability of aquaculture ventures at both smallholder and industrial levels (Barragán-Longoria et al., 2025). The global market's growing reliance on carp as an accessible and dependable protein source has intensified the push for more sustainable farming methods. Its ability to tolerate variable water quality conditions aligns well with the operational demands of modern, high-density rearing technologies (Wang et al., 2024). Nonetheless, intensification brings with it the issue of nitrogenous waste buildup, particularly ammonia, which can impair water quality and, in turn, compromise fish growth, health, and survival. Ammonia accumulation remains one of the principal bottlenecks in maximizing the efficiency of aquaculture production systems (Nguyen-tiêt et al., 2025). Furthermore, the declining availability of land suitable for conventional pond aquaculture, especially in urbanized and heavily populated areas, presents additional obstacles to expanding carp production (Wu et al., 2025). Addressing these limitations calls for robust water quality control approaches, particularly the implementation of recirculating aquaculture systems (RAS), which offer a sustainable path forward for ensuring the health and productivity of common carp farming.

In response to issues like deteriorating water quality and the scarcity of land suitable for aquaculture, Recirculating Aquaculture Systems (RAS) have become a preferred modern alternative that emphasizes sustainability (Akbar et al., 2025a). These systems function through a closed-loop mechanism in which water is continuously filtered, treated, and reused, leading to a substantial decrease in the need for freshwater inputs while ensuring that key water quality parameters remain within optimal ranges (Wu et al., 2025). The performance of RAS can be further improved by integrating advanced filtration media, such as activated carbon, which effectively eliminates toxic ammonia and other waste by-products from fish metabolism, thereby fostering a healthier and more stable aquatic environment (J. Xu et al., 2024**).** Nonetheless, while various filtration materials such as zeolite and biochar have shown promise in ammonia removal (Zhou et al., 2024; Angellinnov et al., 2025), the use of coconut husk-derived activated carbon remains underexplored in

* Corresponding author.; e-mail: saidaliakbar@usk.ac.id.

aquaculture applications, particularly in RAS. For common carp (*Cyprinus carpio*), which can be highly sensitive to poor water quality in intensive culture conditions, the implementation of RAS offers a practical means of supporting higher stocking densities without compromising welfare. In addition, RAS promotes optimal use of available resources, offering a practical solution for regions facing limitations in land availability and freshwater supply. As the aquaculture sector increasingly emphasizes sustainability and environmental responsibility, integrating RAS with effective water treatment technologies represents a promising approach to enhancing common carp production while mitigating ecological impacts.

In a Recirculating Aquaculture System (RAS), ensuring high water quality involves the coordinated application of biological, physical, and chemical filtration techniques. The biological component utilizes nitrifying bacteria, such as Nitrosomonas and Nitrobacter, to biologically oxidize toxic ammonia into relatively safer nitrate. Physical filtration functions to eliminate suspended solids and particulates from the system. Meanwhile, chemical filtration is essential for removing dissolved contaminants, including nitrogen-based compounds like ammonia, by using adsorptive media such as zeolites (Zhou et al., 2024), ion-exchange resins (Liu et al., 2023), and activated carbon (Rehan et al., 2024). Among these, activated carbon is widely valued for its exceptional adsorption capacity and extensive surface area. Traditionally produced from coconut shells (Haider et al., 2025), rice husks (Angellinnov et al., 2025), or sawdust (Yang et al., 2025), activated carbon can also be derived from coconut husk, an abundant and underutilized agricultural byproduct (Akbar et al., 2025b). Utilizing coconut husk to produce activated carbon offers a sustainable and cost-effective alternative, aligning with circular economy principles and reducing organic waste. Despite these advantages, the application of coconut husk-based activated carbon in RAS systems has not been extensively studied or benchmarked against conventional media (Akbar et al., 2025c). The incorporation of coconut husk-derived activated carbon into RAS enhances water purification, supports fish health, and minimizes environmental impacts, thereby contributing to more efficient and sustainable aquaculture practices.

The utilization of coconut husk as a raw material for synthesizing activated carbon in Recirculating Aquaculture Systems (RAS) offers promising advantages. Owing to its abundant lignocellulosic content, namely cellulose, hemicellulose, and lignin, this agricultural residue serves as an excellent carbon-rich substrate that facilitates the formation of well-developed porous networks during the activation stage (Wijaya et al., 2025). The natural abundance and renewability of coconut husk make it an attractive alternative for sustainable filtration media (Fatmawati et al., 2023). Activated carbon produced from coconut husk exhibits favorable adsorption properties, characterized by a well-developed porous network and the presence of functional groups such as hydroxyl (-OH), carbonyl (C=O), and aromatic structures, which enhance surface reactivity (Salaenoi et al., 2024). These attributes facilitate the effective adsorption of nitrogenous wastes, particularly ammonia, making coconut husk-derived activated carbon a promising component in chemical filtration within RAS. By integrating this material into the system, water quality can be significantly improved through the efficient removal of toxic metabolic byproducts, thereby promoting healthier fish growth and enhancing overall system performance. Moreover, the valorization of coconut husk into activated carbon supports sustainable waste management practices, transforming an abundant agricultural byproduct into a high-value filtration material. Nevertheless, the lack of comprehensive data on the comparative effectiveness of coconut husk-based carbon in real RAS conditions constitutes a notable research gap. Therefore, this study aims to evaluate the performance of NaOH-activated carbon derived from coconut husk in improving water quality and physiological responses of *Cyprinus carpio* cultured in a RAS.

2. Materials and Methods

2.1. Collection of coconut husk waste and synthesis of activated carbon

Coconut husk waste used in this study was sourced from traditional markets in the Kuta Alam region of Banda Aceh, Indonesia (coordinates: 5°33'45.0"N 95°20'36.5"E). To ensure cleanliness, the husks underwent thorough washing to eliminate surface impurities, followed by natural sun-drying for three consecutive days to lower their moisture content. Carbonization was performed at 300°C for a duration of two hours, adapting the procedure reported by Yuliusman et al. (2020). The resulting biochar was then pulverized and passed through a 100-mesh sieve for subsequent physicochemical analyses, while a portion was retained in its coarse form for application as filter material. The carbon activation process involved immersion in a sodium hydroxide solution with a 1:4 (w/v) ratio for 24 hours at ambient temperature, as described by Yuliusman et al. (2020). Post-activation, the sample was sequentially rinsed using 1 M hydrochloric acid and deionized water until a neutral pH was achieved. Finally, the activated carbon was oven-dried at 110°C for 12 hours to remove residual moisture.

2.2. Physicochemical and surface characterization of sctivated carbon

To assess the physicochemical characteristics of the synthesized activated carbon, several instrumental analyses were employed. Surface morphology was visualized using a Scanning Electron Microscope (SEM, Hitachi SU3500), with samples mounted on conductive carbon tape. Crystallographic features were determined through X-ray diffraction analysis (XRD, Bruker D8 Advance) utilizing Cu Kα radiation (λ = 1.540598 Å), operated at 30 kV and 15 mA, over a 2θ range of 5° to 80°. Functional groups present on the adsorbent surface were identified using Fourier Transform Infrared Spectroscopy (FTIR, Thermo Nicolet iS50), scanning in the spectral region of 500–4000 cm^{-1}. The porosity and surface area were evaluated via nitrogen adsorption–desorption isotherms at 77 K using a Quadrasorb-Evo instrument. The Brunauer–Emmett–Teller (BET) method was applied to estimate the specific surface area, while the total pore volume was calculated at a relative pressure (P/P_0) close to 0.99.

2.3. Collection and acclimatization of common carp

A total of 200 juvenile common carp (*Cyprinus carpio*), measuring between 3.12 and 3.45 cm in length and weighing 0.24 to 0.289 g, were sourced from Glory Pulo Nusa hatchery in Lambaro, Aceh Besar, Indonesia. According to the supplier, the fish had not been exposed to any antibiotics or chemical treatments during cultivation. Upon arrival at the experimental site, the fish underwent a 7-day acclimation period in plastic tanks measuring 60 × 40 × 40 cm^3, during which their health status and behavior were monitored daily (Akbar et al., 2025d). Throughout this period, they were provided with a commercial feed containing 40% crude protein, administered to apparent satiation three times daily at 09:00, 12:00, and 17:00.

2.4. Experimental aetup of the Recirculating Aquaculture System (RAS)

The RAS experimental design comprised five distinct treatment groups, each replicated four times. The treatments differed by the amount of activated carbon applied: the control group (P1) received no carbon, while P2, P3, P4, and P5 were administered 5 g, 10 g, 15 g, and 20 g of activated carbon, respectively, guided by the methodology of Prastiawan et al. (2019). The trials were conducted in 27-liter cylindrical plastic tanks (dimensions: 35 × 31 × 60 cm), each filled with 20 liters of sterilized tap water and continuously aerated to maintain sufficient dissolved oxygen concentrations. Each tank was stocked with ten juvenile *Cyprinus carpio*. Fish were fed a high-protein commercial diet (40% crude protein) at 5% of their body weight, delivered in three daily feedings at 09:00, 12:00, and 17:00 (Prastiawan et al., 2019). The experiment was conducted over a 28-day period without any water renewal. Weekly monitoring was conducted for key water parameters, including temperature, pH, and dissolved oxygen (DO). Throughout the study, the water temperature remained within 24–26°C, pH between 8.2–8.6, and DO ranged from 5.0 to 7.4 mg/L. This configuration facilitated a systematic assessment of the effects of varying activated carbon dosages on water quality enhancement and fish performance under RAS conditions.

2.5. Determination of ammonia levels in RAS water

To evaluate the concentration of ammonia in the recirculating aquaculture system, water samples (10 mL) were systematically collected from each of the 20 tanks, ensuring comprehensive representation of water conditions. The analysis utilized the indophenol blue technique, wherein specific reagents were introduced to the samples to induce the formation of an indophenol chromophore. The reaction mixture was then incubated for 30 minutes at room temperature to allow complete color development. After incubation, absorbance readings were taken at a wavelength of 640 nm using a UV-Vis spectrophotometer, corresponding to the maximum absorption of the developed indophenol complex (Jain et al., 2021). Ammonia concentrations were quantified in parts per million (ppm) using a standard calibration curve derived from known ammonia solutions.

2.6. Measurement of oxidative stress biomarkers

To evaluate oxidative stress in fish, serum samples were analyzed using ELISA-based commercial kits from Elabscience, targeting key oxidative stress biomarkers. Total Superoxide Dismutase (T-SOD) activity was measured in units per milliliter (U/mL) using the WST-1 Method Kit (Cat. No. E-BC-K020-M), while Catalase (CAT) activity was expressed in units per milliliter (U/mL) based on the hydrogen peroxide decomposition rate (Cat. No. E-BC-K031-S). Glutathione S-transferase (GST) activity was determined using the GST Activity Assay Kit (Cat. No. E-BC-K278-S) and expressed as units per liter (U/L). Lipid peroxidation was assessed through malondialdehyde (MDA) levels, measured in micromoles per liter (µmol/L) using the TBA-based MDA Colorimetric Assay Kit (Cat. No. E-BC-K025-M). All assays were performed in accordance with the manufacturer's instructions, and the results were reported as enzyme activities or MDA concentration per volume of serum.

2.7. Measurement of respiratory responses

Opercular beat rate (OBR) and oxygen consumption rate (OCR) were measured to assess respiratory responses of the fish (Kim et al., 2025). OBR was determined by visually counting the opercular movements of individual fish for one minute while the fish remained undisturbed in the experimental tanks. The counting was repeated four times per fish**,** and the average value was recorded in beats per minute (bpm). For OCR measurement, individual fish were transferred to sealed respirometry chambers filled with aerated experimental water. Dissolved oxygen concentrations were measured at the start and after a fixed incubation period of 1 hour using a calibrated dissolved oxygen meter (mg O_2/L). Oxygen consumption was calculated based on the decline in oxygen concentration, fish body weight, and duration of the incubation, and expressed as milligrams of oxygen consumed per kilogram of body weight per hour (mg O_2/kg/h). All measurements were conducted in quadruplicate (n = 4) to ensure accuracy and reproducibility.

2.8. Measurement of hematological parameters

To assess the hematological status of *Cyprinus carpio*, several blood parameters were evaluated on the 20 day of the trial, including mean corpuscular hemoglobin concentration (MCHC), mean corpuscular hemoglobin (MCH), mean corpuscular volume (MCV), hematocrit (HCT), hemoglobin (Hb), white blood cell (WBC) count, and red blood cell (RBC) count. Blood samples were drawn from the caudal vein of anesthetized fish (n = 4 per treatment) using sterile 1 mL syringes preloaded with EDTA to prevent coagulation (Xu et al., 2021). Hematocrit levels were determined using the microcapillary method: blood was introduced into heparinized tubes, centrifuged at 12,000 rpm for 5 minutes, and the resulting packed cell volume was recorded as a percentage of total volume. Hemoglobin concentration was analyzed via spectrophotometry using the cyanmethemoglobin approach, with readings taken at 540 nm using a Thermo Scientific Genesys 150 UV-Vis spectrophotometer. RBC and WBC counts were conducted using a Neubauer counting chamber viewed under an Olympus CX23 light microscope at 400× magnification. Derived indices, MCV, MCH, and MCHC, were computed from measured values using conventional hematological formulas: MCV (fL) = (HCT × 10) / RBC, MCH (pg) = (Hb × 10) / RBC, and MCHC (g/dL) = (Hb × 100) / HCT.

2.9. Assessment of abnormal erythrocyte morphology

Following the 20-day rearing period, blood was drawn aseptically from the caudal vein of Cyprinus carpio using sterile syringes coated with EDTA to prevent clotting, in accordance with the method described by Bardhan et al. (2024). A fresh drop of blood was promptly spread into a thin layer on a pre-cleaned glass slide to obtain a uniform monolayer. After air-drying, the slides were immersed in absolute methanol for fixation over a 5-minute period. Subsequently, the samples were stained with 10% Giemsa solution for 15 minutes to visualize cellular structures. The slides were then rinsed with distilled water and dried at ambient temperature. Morphological observation of erythrocytes was performed under 1000× magnification using immersion oil and a light microscope to detect possible malformations. Malformation assessment was conducted using a semi-quantitative method by counting 1000 erythrocytes per slide and calculating the percentage of cells exhibiting abnormalities, such as membrane ruptures, irregular shapes, binucleated cells, and cytoplasmic vacuoles. This approach allowed for a standardized comparison of erythrocyte integrity across treatment groups and provided insight into hematological responses to varying dosages of activated carbon.

2.10. Data analysis

All data were processed and visualized using Origin Pro 2024, while statistical evaluations were performed using IBM SPSS Statistics version 26 (Chicago, IL, USA). Descriptive results were expressed as mean values accompanied by standard deviations (mean ± SD). Prior to hypothesis testing, data normality was examined using the Shapiro–Wilk test, and homogeneity of variances was verified using Levene's test. One-way analysis of variance (ANOVA) was applied to determine significant differences among treatments, with pairwise comparisons carried out **using** Duncan's multiple range test. Statistical significance was set at $p < 0.05$.

3. Results

3.1. Physicochemical properties of activated carbon

Based on Table 1, the activated carbon derived from coconut husk and treated with NaOH exhibited a notable improvement in quality. The ash content decreased from 6.34 ± 0.12% to 2.34 ± 0.12%, with both values remaining within the SNI standard limit (≤10%). The moisture content increased from 4.82 ± 0.23% to 6.64 ± 0.54%, while still complying with the SNI standard (≤15%). The methylene blue adsorption capacity improved from 89.54 ± 0.23 mg/g to 132.12 ± 1.23 mg/g, surpassing the minimum SNI requirement (≥120 mg/g) after activation. Additionally, the iodine number increased from 687.43 ± 2.66 mg/g to 992.95 ± 3.41 mg/g, exceeding the SNI threshold (≥750 mg/g). The specific surface area, as determined by BET analysis, also increased from 323.12 ± 5.12 m^2/g to 654.43 ± 5.23 m^2/g, indicating an enhancement in the active surface area following the activation process.

Table 1. Physicochemical properties of activated carbon from coconut husk (n = 3)

No	Parameter	Carbon Before Activation	Carbon After Activation	SNI Standard
1	Ash Content (%)	6.34 ± 0.12	2.34 ± 0.12	≤ 10
2	Moisture Content (%)	4.82 ± 0.23	6.64 ± 0.54	≤ 15
3	Methylene Blue Adsorption Capacity (mg/g)	89.54 ± 0.23	132.12 ± 1.23	≥ 120
4	Iodine Number (mg/g)	687.43 ± 2.66	992.95 ± 3.41	≥ 750
5	BET Surface Area (m^2/g)	323.12 ± 5.12	654.43 ± 5.23	-

*Indonesian National Standard 06–3730-1995

3.2. Morphological and structural characterization of coconut husk-derived activated carbon

Based on Figure 1, SEM images revealed notable changes in the surface morphology of activated carbon before and after the activation process. Prior to activation (Figure 1a), the carbon surface appeared relatively dense with a compact structure and a limited number of pores. Following activation (Figure 1c), the surface morphology became more open and porous, indicating an increase in both pore number and pore size. The pore size distribution graph (Figure 1b) showed that before activation, the average pore diameter was 398.4306 µm, predominantly within the 300–350 µm range. After activation, as shown in Figure 1d, the average pore diameter significantly increased to 847.6096 µm, with the pore size distribution shifting towards larger diameters, particularly within the 700–900 µm range. These changes indicate that the activation process effectively enlarged the pore size and significantly enhanced the porosity of the activated carbon structure.

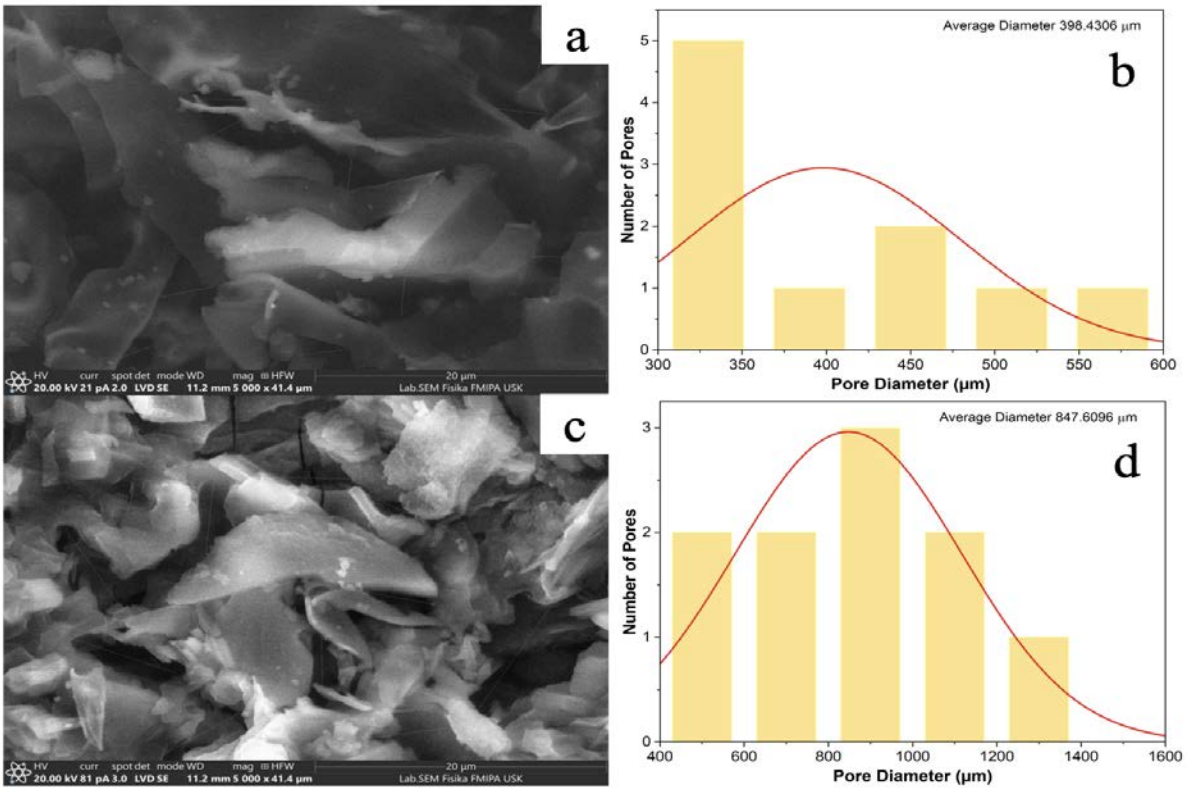

Figure 1. SEM images and pore size distribution of activated carbon: (a) morphology before activation, (b) pore size distribution before activation, (c) morphology after activation, (d) pore size distribution after activation.

According to Figure 2a, the XRD diffraction patterns of the carbon exhibited broad peaks, indicating an amorphous structure within the 2θ range of approximately 20°–30°, both before and after activation. However, a decrease in diffraction intensity was observed following activation, suggesting disruptions in the graphitic structural order induced by the activation treatment. In Figure 2b, the FTIR spectra displayed changes in intensity and shifts in wavenumbers for several functional groups. The wavenumber range of 3682–3050 cm^{-1} prior to activation shifted to 3695–2984 cm^{-1} post-activation, corresponding to O–H stretching vibrations. Other shifts included the C=O stretching band from 1712 cm^{-1} to 1692 cm^{-1}, and the aromatic C–C ring stretching band from 1596 cm^{-1} to 1554 cm^{-1}. Additionally, the C–H rocking band shifted from 1375 cm^{-1} to 1312 cm^{-1}, and the C–O stretching band shifted from 1102 cm^{-1} to 1151 cm^{-1}. Table 4.2 supports these findings by summarizing the observed wavenumber shifts and the corresponding functional group vibrations identified through FTIR analysis, indicating that the activation process altered the surface chemical composition of the carbon and enhanced the presence of oxygen-containing functional groups.

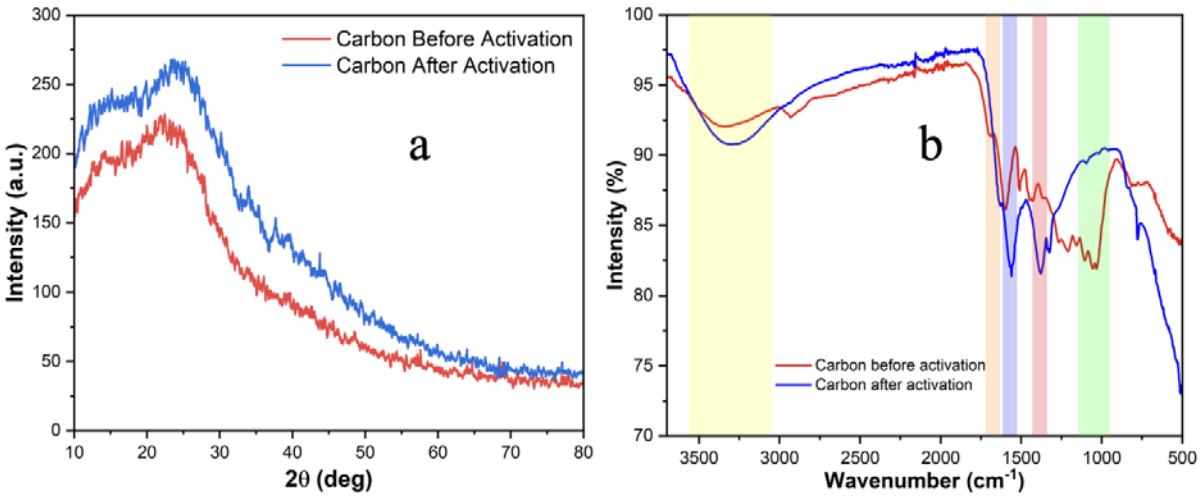

Figure 2. (a) XRD diffraction patterns of carbon before and after activation; (b) FTIR spectra of carbon before and after activation.

3.3. Ammonia concentration in common carp culture media

Based on Table 2, the use of coconut husk-derived activated carbon as a filter in the RAS for common carp culture had a significant effect on ammonia concentration ($p < 0.05$) on both Day 10 and Day 20. The mean ammonia concentration on Day 10 decreased from 0.0096 ± 0.0006 ppm in P1 (without activated carbon) to 0.0071 ± 0.0004 ppm in P5 (20 g dose). A similar trend was observed on Day 20, with the highest ammonia concentration recorded in P1 at 0.0178 ± 0.0013 ppm and the lowest in P5 at 0.0103 ± 0.0006 ppm. All values in treatments P3, P4, and P5 were below the threshold set by Government Regulation (GR) No. 82 of 2001 (<0.02 ppm), and substantially lower than the limits established by the WHO (1.5 ppm) and the EPA (0.25–32.5 ppm). Post-hoc analysis revealed significant differences among treatments, with higher doses of activated carbon resulting in greater reductions in ammonia concentration. Treatment P5 demonstrated the highest effectiveness in lowering ammonia levels compared to the other treatments.

Tabel 2. Ammonia concentration (ppm) on day 10 and day 20 for each treatment (n = 4)

Treatment	Ammonia concentration (ppm)		Threshold limit (ppm)		
	Day 10	Day 20	WHO	EPA	PP
P1	0.0096 ± 0.0006^{c}	0.0178 ± 0.0013^{d}	1.5	0.25–32.5	< 0.02
P2	0.0085 ± 0.0002^{b}	0.0154 ± 0.0015^{c}			
P3	0.0076 ± 0.0003^{a}	0.0125 ± 0.0009^{b}			
P4	0.0074 ± 0.0003^{a}	0.0116 ± 0.0008^{bc}			
P5	0.0071 ± 0.0004^{a}	0.0103 ± 0.0006^{a}			

World Health Organization (WHO)
Environmental Protection Agency (EPA)
Government Regulation (GR) No. 82 of 2001 on Water Quality Management and Water Pollution Control

3.4. Oxidative stress biomarkers in common carp under different activated carbon treatments

The activities of oxidative stress biomarkers, including superoxide dismutase (SOD), catalase (CAT), glutathione S-transferase (GST), and malondialdehyde (MDA), are presented in Figure 3. Significant differences ($p < 0.05$) were observed across treatments (P1–P5) and sampling days (Day 0, Day 10, and Day 20). SOD activity (Figure 3a), expressed in Unit/mL, showed a time-dependent increase in all treatments, with the highest value recorded in P1 on Day 20 (23.775 U/mL) and the lowest in P5 on Day 0 (8.575 U/mL). CAT activity (Figure 3b), also in Unit/mL, followed a similar trend, peaking in P1 on Day 20 (0.4705 U/mL) and reaching the lowest point in P5 on Day 0 (0.09125 U/mL). For GST activity (Figure 3c), measured in Unit/L, values were consistently higher in P1 and P2, particularly on Day 10 (13.875 and 12.875 U/L, respectively), but declined on Day 20 in all groups, especially in P5 (5.25 U/L). In contrast, MDA activity (Figure 3d), expressed in µmol/L, was highest in P1 (4.95 µmol/L) and progressively decreased in treatments with more effective filtration, with the lowest value recorded in P5 on Day 20 (1.3 µmol/L).

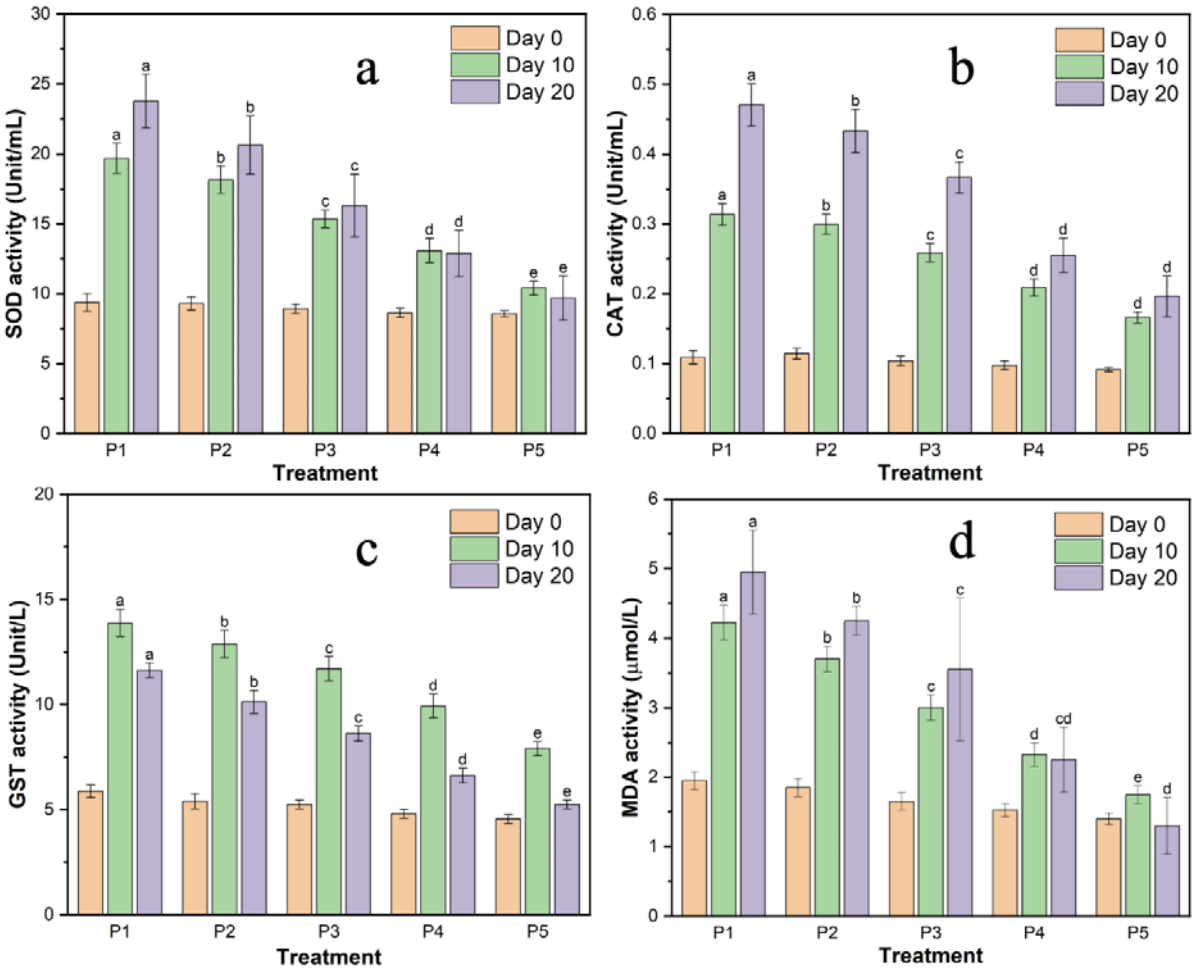

Figure 3. Activities of oxidative stress biomarkers in *Cyprinus carpio* cultured under different activated carbon treatments: (a) superoxide dismutase (SOD), (b) catalase (CAT), (c) glutathione S-transferase (GST), and (d) malondialdehyde (MDA). Data are presented as mean ± SD (n = 4) at Day 0, Day 10, and Day 20. Different letters indicate significant differences ($p < 0.05$) among treatments and sampling days.

3.5. Respiratory responses of common carp under different activated carbon treatments

Respiratory responses, including opercular beat rate (OBR) and oxygen consumption rate (OCR), under different activated carbon treatments are presented in Figure 4. OBR (Figure 4a) exhibited significant differences ($p < 0.05$) across treatments and sampling days. On Day 20, the highest OBR was recorded in P1 (130 ± 4 bpm), while the lowest was observed in P5 (74 ± 3 bpm). A decreasing trend in OBR was evident with increasing activated carbon dosage. Similarly, OCR (Figure 4b) showed significant variation ($p < 0.05$). On Day 20, P1 exhibited the lowest OCR at 85 ± 3 mg O_2/kg/h, whereas P5 demonstrated the highest OCR at 220 ± 4 mg O_2/kg/h. A progressive increase in OCR was observed with higher activated carbon dosages, indicating enhanced respiratory efficiency. Overall, these results reflect clear differences in respiratory parameters among treatments over time.

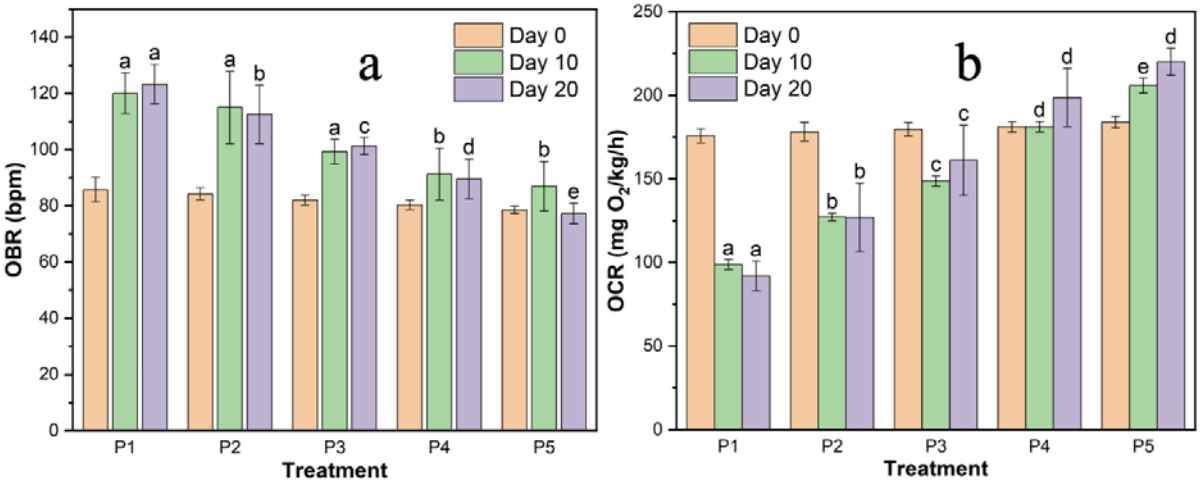

Figure 4. Respiratory responses of Cyprinus *carpio* cultured under different activated carbon treatments: (a) opercular beat rate (OBR, bpm), (b) oxygen consumption rate (OCR, mg O_2/kg/h). Data are presented as mean ± SD (n = 4) at Day 0, Day 10, and Day 20. Different letters indicate significant differences ($p < 0.05$) among treatments and sampling days.

3.6. Hematological parameters of common carp under different activated carbon treatments

Hematological parameters of *Cyprinus carpio* cultured under different activated carbon treatments are presented in Table 3. Significant differences ($p < 0.05$) were observed across treatments for all measured parameters. The mean corpuscular hemoglobin concentration (MCHC) increased progressively from 27.87 ± 1.57 g/dL in P1 to 33.52 ± 0.24 g/dL in P5. Mean corpuscular hemoglobin (MCH) also showed a notable increase, from 82.70 ± 2.21 pg in P1 to 109.90 ± 1.14 pg in P5. Similarly, mean corpuscular volume (MCV) rose from 212.50 ± 15.54 fL in P1 to 362.50 ± 29.01 fL in P5. Hematocrit values ranged from 26.20 ± 0.54% in P1 to 39.87 ± 3.15% in P5, indicating improved hematological status with increasing activated carbon dosage. Hemoglobin concentration increased from 6.12 ± 0.61 g/dL in P1 to 10.37 ± 1.82 g/dL in P5. Conversely, white blood cell (WBC) count decreased significantly, from 138.75 ± 5.37 ×10³/μL in P1 to 52.5 ± 5.25 ×10³/μL in P5, suggesting a reduction in physiological stress. Red blood cell (RBC) count increased from 1.15 ± 0.16 ×10⁶/μL in P1 to 2.08 ± 0.02 ×10⁶/μL in P5. These results indicate marked hematological improvements associated with higher activated carbon dosages.

Table 3. Hematological parameters of *Cyprinus carpio* cultured under different activated carbon treatments.

Parameters	P1	P2	P3	P4	P5
MCHC (g/dL)	27.87 ± 1.57^{a}	29.05 ± 0.31^{a}	30.57 ± 0.33^{b}	31.97 ± 0.91^{c}	33.52 ± 0.24^{d}
MCH (pg)	82.70 ± 2.21^{a}	88.87 ± 1.18^{d}	95.90 ± 1.01^{c}	102.02 ± 1.02^{d}	109.90 ± 1.14^{e}
MCV (fL)	212.50 ± 15.54^{a}	242.50 ± 11.90^{a}	275.75 ± 31.92^{b}	317.50 ± 6.45^{c}	362.50 ± 29.01^{d}
Hematokrit (%)	26.20 ± 0.54^{a}	29.20 ± 2.87^{a}	34.17 ± 2.95^{b}	36.37 ± 0.50^{bc}	39.87 ± 3.15^{c}
Hemoglobin (g/dL)	6.12 ± 0.61^{a}	7.72 ± 0.99^{ab}	8.57 ± 0.37^{bc}	9.65 ± 0.93^{cd}	10.37 ± 1.82^{d}
WBC (10³/μL)	138.75 ± 5.37^{a}	106.25 ± 9.46^{b}	98.75 ± 4.34^{c}	76.25 ± 9.25^{c}	52.5 ± 5.25^{d}
RBC (10⁶/μL)	1.15 ± 0.16^{a}	1.30 ± 0.13^{a}	1.60 ± 0.16^{b}	1.90 ± 0.20^{c}	2.08 ± 0.02^{c}

Note: Different superscript letters in the table indicate significant differences between treatments. Values are presented with standard deviations (n = 4). In this study, activated carbon was applied at different doses: P1 (control), P2 (5 g), P3 (10 g), P4 (15 g), and P5 (20 g).

3.7. Effects of ammonia reduction on erythrocyte morphology

The types and intensities of erythrocyte malformations observed in *Cyprinus carpio* under different activated carbon treatments are shown in Figure 5 and Table 4. Various morphological abnormalities were detected, including vacuolated cells, hemolyzed cells, lacerated membranes, binucleated cells, double cells, deformed cells, and swollen cells.

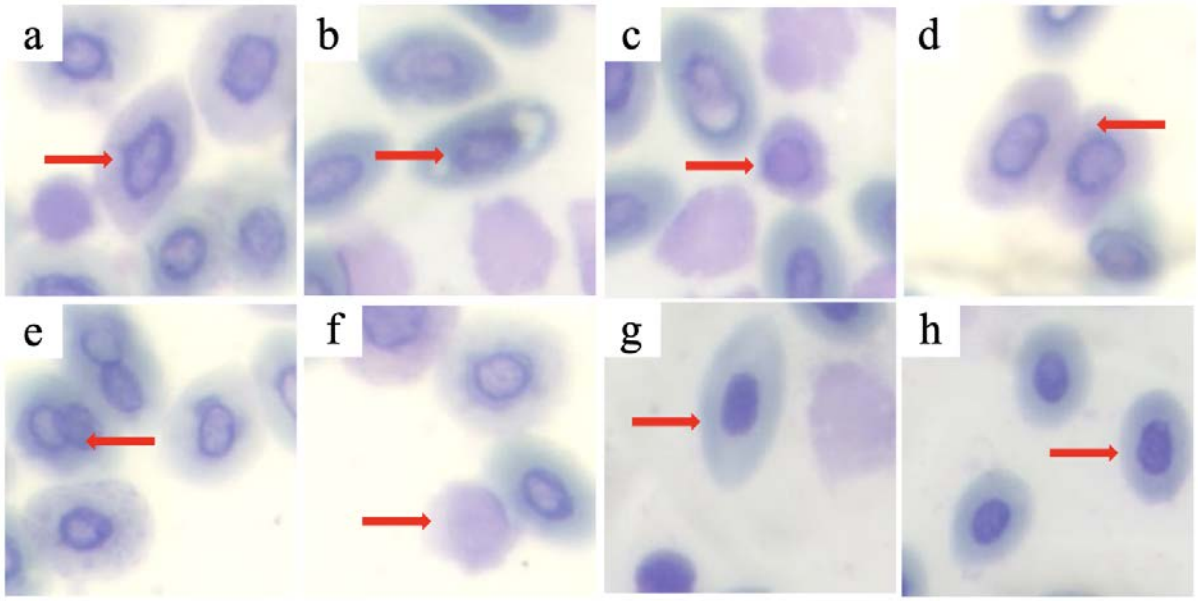

Figure 5. Appearance of erythrocyte malformations in *Cyprinus carpio* under different treatment conditions (P1–P5). (a) Deformed cell (P1), (b) Lacerated membrane (P1), (c) Vacuolated cell (P2), (d) Double cell (P3), (e) Binucleus (P3), (f) Hemolyzed cell (P3), (g) Swollen cell (P4), and (h) Normal erythrocyte (P5). Scale bar = 30 µm.

Erythrocyte abnormalities were most prominent in the control group (P1), with severe deformities observed, including pronounced cases of cell distortion, membrane rupture, binucleation, and hemolysis. Swelling and vacuolization were also notable at moderate levels. As the activated carbon dosage increased across treatments, a marked reduction in both frequency and intensity of these malformations was evident. In P2, while some abnormalities remained prominent, particularly deformed and ruptured cells, their severity began to diminish. By P3, the occurrence of abnormal cell types had declined further, with most anomalies classified as mild to moderate. Treatment P4 showed minimal disruptions, where only slight deformities, swelling, and cell fusion persisted, and several malformation types were no longer detected. In the highest carbon treatment (P5), erythrocyte integrity was nearly restored, with only occasional mild swelling and minimal deformation or hemolysis present, and no signs of binucleation, vacuolization, or membrane damage. A noticeable increase in the presence of intact, healthy red blood cells was recorded in this group, supporting the effectiveness of higher activated carbon dosages in mitigating cellular damage.

Table 4. Erythrocyte abnormalities and severity

Type of Malformation	P1	P2	P3	P4	P5
Vacuolated cell	++	+	–	–	–
Hemolyzed cell	+++	++	++	++	+
Lacerated membrane	+++	++	+	–	–
Binucleus	++	+	+	–	–
Double cell	+++	++	+	++	+
Deformed cell	+++	+++	++	++	+
Swollen cell	++	++	++	+	–

Note: None (–), mild (+), moderate (++), and severe (+++)

3.8. Effect of ammonia filtration on survival rate of common carp

The survival rate (SR) of *Cyprinus carpio* varied significantly across treatments ($p < 0.05$), as shown in Table 5. The lowest SR was observed in P1 (67.50 ± 5.00%), while the highest was recorded in P5 (97.50 ± 5.00%). Intermediate SR values were noted in P2 (75.00 ± 5.77%), P3 (85.00 ± 5.77%), and P4 (87.50 ± 5.00%). Increasing activated carbon dosage clearly improved fish survival throughout the culture period.

Table 5. Survival rate (SR) of *Cyprinus carpio* under different activated carbon treatments.

Treatment	*Survival Rate* (SR) (%)
P1	67.50 ± 5.00^{a}
P2	75.00 ± 5.77^{a}
P3	85.00 ± 5.77^{b}
P4	87.50 ± 5.00^{b}
P5	97.50 ± 5.00^{c}

Note: Different superscript letters in the table indicate significant differences between treatments. Values are presented with standard deviations (n = 4). In this study, activated carbon was applied at different doses: P1 (control), P2 (5 g), P3 (10 g), P4 (15 g), and P5 (20 g).

4. Discussion

The physicochemical characteristics of the activated carbon derived from coconut husk and modified with NaOH treatment demonstrated substantial improvements in adsorption performance and structural properties (Table 1). The significant reduction in ash content and the controlled moisture level suggest enhanced material purity and stability, both of which comply with the Indonesian National Standard (SNI). The marked increase in methylene blue adsorption capacity, from 89.54 to 132.12 mg/g, highlights the improvement in mesoporous structure, while the substantial rise in iodine number, exceeding 992 mg/g, indicates an elevated microporous surface conducive for efficient adsorption processes. This enhancement is further corroborated by the two-fold increase in specific surface area as measured by BET analysis. These findings align with previous studies where NaOH activation was

reported to promote the development of well-defined pore structures and increased surface area in biomass-derived activated carbons (Huno et al., 2023; Kasmuri et al., 2022). However, unlike prior reports utilizing wood-based or synthetic precursors, the present study uniquely employs coconut husk, a readily available and underutilized agricultural waste in tropical regions, thus providing a more sustainable and cost-effective alternative (Fu et al., 2020). The combination of high adsorption capacity, large surface area, and compliance with SNI standards underscores the suitability of this activated carbon for advanced water treatment applications, particularly for ammonia filtration in aquaculture systems. The novelty of this study lies not only in the effective valorization of coconut husk waste but also in demonstrating the synergistic effect of NaOH activation in enhancing the adsorption properties beyond commonly reported values, positioning this material as a highly competitive option in sustainable aquaculture water management.

The SEM analysis (Figure 1) revealed significant morphological transformations of the activated carbon following the NaOH activation process. Prior to activation (Figure 1a), the carbon surface exhibited a dense, compact morphology with relatively few pores, indicating limited surface accessibility. After activation (Figure 1c), the surface became notably more porous and irregular, suggesting the effective removal of volatile components and structural rearrangement induced by chemical activation (Huno et al., 2023). Correspondingly, the pore size distribution shifted markedly. Before activation (Figure 1b), the average pore diameter was 398.43 µm, predominantly within the 300–350 µm range, indicative of a relatively narrow distribution of smaller pores. Post-activation (Figure 1d), the average pore diameter increased significantly to 847.61 µm, with a broader distribution skewed towards larger pores (700–900 µm range). This substantial enlargement of pore size and increase in porosity is consistent with previous findings where alkali activation facilitated pore development through etching and widening of pre-existing pore structures (Ajien et al., 2022; Armstrong et al., 2014). The observed morphological evolution enhances the material's adsorption capacity by increasing the available surface area and improving diffusion pathways. Notably, the average pore diameter achieved in this study surpasses several reported values for biomass-derived activated carbons, underscoring the effectiveness of the employed NaOH activation protocol in tailoring pore architecture for advanced adsorption applications (Tomy et al., 2024).

The XRD and FTIR analyses provide crucial insights into the structural and chemical modifications induced by the NaOH activation process on coconut husk-derived carbon (Figure 2). The XRD patterns (Figure 2a) exhibited broad diffraction peaks within the 2θ range of 20°–30°, both before and after activation, characteristic of an amorphous carbon structure with disordered graphitic domains. Notably, a decrease in diffraction intensity post-activation indicates further disruption of the graphitic lattice, likely due to chemical etching and pore development (Armstrong et al., 2014; Tomy et al., 2024). These structural changes are consistent with the observed increase in surface area and porosity reported earlier (Armstrong et al., 2014). The FTIR spectra (Figure 2b) revealed substantial shifts in functional groups following activation. The broad O–H stretching band shifted from 3682–3050 cm^{-1} to 3695–2984 cm^{-1}, indicating enhanced surface hydroxylation (Fu et al., 2020). The C=O stretching band shifted from 1712 cm^{-1} to 1692 cm^{-1}, suggesting modification of carbonyl functionalities. Additionally, shifts in aromatic C–C (1596 → 1554 cm^{-1}), C–H rocking (1375 → 1312 cm^{-1}), and C–O stretching (1102 → 1151 cm^{-1}) bands further confirm the introduction of oxygen-containing groups during activation (Tomy et al., 2024). These functional groups enhance the carbon's hydrophilicity and adsorption capacity, facilitating effective ammonia removal in RAS applications. Overall, the combined XRD and FTIR findings corroborate the morphological and chemical transformations that underpin the superior filtration performance of the activated carbon produced in this study.

The application of coconut husk-derived activated carbon in the recirculating aquaculture system (RAS) demonstrated a significant impact on ammonia reduction in *Cyprinus carpio* culture (Table 2). Ammonia concentration consistently decreased with increasing activated carbon doses on both Day 10 and Day 20 ($p < 0.05$), indicating enhanced filtration efficiency. The lowest ammonia levels were observed in P5 (20 g carbon), achieving reductions of approximately 26% on Day 10 and 42% on Day 20 compared to the control. Importantly, ammonia concentrations in treatments P3, P4, and P5 remained well below regulatory thresholds established by GR No. 82/2001, WHO, and EPA, ensuring a safe environment for fish culture. This trend confirms the efficacy of biomass-based activated carbon in improving water quality in aquaculture systems (Hamid, Humaidi, et al., 2024; Hamid, Nasution, et al., 2024). However, the current study demonstrates superior ammonia removal performance compared to previous works utilizing coconut shell- or bamboo-based carbons, likely due to the optimized pore structure and increased surface area of the NaOH-activated coconut husk carbon (Han et al., 2021). Furthermore, the gradual improvement from Day 10 to Day 20 suggests a sustained filtration capacity and adsorption stability over time. The findings highlight the potential of this low-cost, sustainable material for effective ammonia management in RAS, contributing to improved fish health and system sustainability.

The dynamics of oxidative stress biomarkers in the gills of *Cyprinus carpio* under different activated carbon treatments are depicted in Figure 3. The observed variations in SOD, CAT, GST, and MDA activities reflect the physiological responses of gill tissues to ammonia exposure and the mitigating effects of activated carbon filtration. SOD and CAT activities showed progressive increases across all treatments and sampling days, with the highest activities recorded in P1 on Day 20, indicating heightened superoxide radical and hydrogen peroxide detoxification under elevated ammonia stress. These trends align with prior studies (Koner et al., 2021b; Zhao et al., 2021) reporting enhanced SOD and CAT activities in fish exposed to oxidative stressors. In contrast, GST activity displayed a biphasic response, an initial increase up to Day 10, followed by a decline on Day 20. This pattern suggests early-phase compensatory activation of GST, which subsequently diminished due to glutathione depletion and compromised antioxidant capacity under prolonged

ammonia exposure (Kumar et al., 2023; Mohamed et al., 2020). MDA levels exhibited a steady increase over time, particularly in P1 and P2, reflecting the extent of lipid peroxidation and membrane damage induced by oxidative stress (Dawood et al., 2022). Notably, treatments with higher activated carbon doses (P3–P5) consistently demonstrated lower oxidative biomarker activities, indicating effective ammonia removal and improved oxidative balance in gill tissues. Compared to previous reports utilizing other filtration media, the coconut husk-derived activated carbon in this study provided superior protection against oxidative stress, as evidenced by the lower MDA accumulation and moderated antioxidant enzyme responses (Dawood et al., 2022; Qin et al., 2023). These findings underscore the critical role of optimized bio-based filtration strategies in safeguarding fish health within recirculating aquaculture systems.

The respiratory responses of *Cyprinus carpio* reflected distinct physiological adaptations to ammonia stress and the efficacy of activated carbon filtration (Figure 4). The observed reduction in opercular beat rate (OBR) with increasing activated carbon dosage suggests improved water quality and reduced metabolic stress. Higher OBR values in P1 and P2 align with elevated ammonia levels, necessitating increased ventilatory effort for gas exchange, consistent with prior observations in stressed fish (X.-N. Xu et al., 2022). Conversely, oxygen consumption rate (OCR) increased progressively with activated carbon dosage, with P5 exhibiting the highest OCR, indicative of enhanced respiratory efficiency under improved environmental conditions. This pattern underscores the role of adequate filtration in supporting aerobic metabolism and overall fish performance (Pei et al., 2021; Zhang et al., 2023). These findings highlight the potential of sustainable filtration strategies in optimizing fish health and welfare.

The hematological responses of *Cyprinus carpio* to different activated carbon treatments provide valuable insights into fish health and physiological adaptation within the RAS (Table 3). Progressive increases in MCHC, MCH, MCV, hematocrit, and hemoglobin concentrations with higher activated carbon dosages indicate improved erythropoietic activity and enhanced oxygen transport capacity. These improvements are likely linked to the reduction of ammonia-induced stress and oxidative damage, as better water quality supports hematopoietic processes and membrane integrity (Chen & Luo, 2023; Witeska et al., 2023). The decline in WBC counts from P1 to P5 suggests a reduction in systemic stress and immune activation, which typically elevate leukocyte levels under unfavorable environmental conditions (Ahmed et al., 2020). The observed increase in RBC counts across treatments further reflects improved erythropoiesis and oxygen-carrying capacity, supporting enhanced metabolic performance. These findings align with those of (Hoque & Das, 2025), who reported improved hematological profiles in fish exposed to optimized water quality in RAS systems. Notably, the current study demonstrates superior hematological outcomes compared to previous works utilizing conventional filtration, underscoring the effectiveness of coconut husk-derived activated carbon. The optimized pore structure and high adsorption capacity of the activated carbon likely contributed to efficient ammonia removal, thereby mitigating hemolytic and oxidative stress in fish. Collectively, the hematological improvements observed in this study highlight the critical role of advanced filtration strategies in promoting fish health and welfare in intensive aquaculture settings.

The analysis of erythrocyte malformations in *Cyprinus carpio* under different activated carbon treatments revealed a clear dose-dependent trend in morphological abnormalities (Figure 5, Table 4). Fish reared without activated carbon (P1) exhibited the highest frequency and severity of erythrocyte malformations, including severe deformations, double cells, lacerated membranes, and hemolyzed cells, reflecting substantial cellular stress and membrane instability likely induced by elevated ammonia levels and associated oxidative stress. This finding is consistent with reports by Khatun et al., (2021) and Zhong & Yan, (2025), who observed similar erythrocyte damage under polluted or toxic aquatic conditions. As the dosage of activated carbon increased (P2–P5), a progressive reduction in both the number and severity of erythrocyte abnormalities was evident, culminating in predominantly normal erythrocyte morphology in P5, where only mild residual malformations persisted. The reduction in malformations parallels the improvements observed in water quality and oxidative stress parameters, suggesting that activated carbon filtration effectively mitigated environmental stressors that compromise erythrocyte integrity. Notably, the absence of binucleated, lacerated, and vacuolated cells in P5 highlights the protective role of optimized filtration in maintaining cellular homeostasis. These results underscore the sensitivity of erythrocyte morphology as a biomarker for sub-lethal stress in fish and reinforce the superior performance of coconut husk-derived activated carbon in promoting hematological stability.

The survival rate (SR) of *Cyprinus carpio* exhibited a clear dose-dependent improvement with increasing activated carbon levels (Table 5), complementing the physiological and hematological enhancements observed in this study. The lowest SR in P1 (67.50%) corresponds with elevated ammonia concentrations, heightened oxidative stress markers, compromised hematological profiles, and severe erythrocyte malformations reported earlier. Conversely, the highest SR in P5 (97.50%) aligns with reduced ammonia levels, stabilized oxidative biomarkers, improved blood parameters, and minimal erythrocyte abnormalities, indicating a well-maintained internal environment conducive to fish survival. These findings corroborate reports by Akbar et al. (2025), emphasizing the critical role of water quality in determining fish health and survival. The superior performance of coconut husk-derived activated carbon demonstrated here underscores its potential as a sustainable filtration solution in RAS. Overall, the integration of physiological, hematological, and survival data highlights the material's efficacy in enhancing fish welfare and system sustainability.

5. Conclusions

This study demonstrated that coconut husk-derived activated carbon effectively improved water quality and fish health in a recirculating aquaculture system (RAS) for *Cyprinus carpio*. NaOH activation significantly enhanced the physicochemical properties of the carbon, including

surface area and pore structure, thereby increasing its ammonia adsorption capacity. The application of activated carbon resulted in substantial reductions in total ammonia nitrogen, with P5 (20 g carbon) maintaining levels well below regulatory thresholds. Improved water quality was reflected in decreased oxidative stress, as evidenced by reduced SOD, CAT, GST, and MDA activities in gill tissues under higher carbon dosages. Concurrently, hematological parameters improved, with increases in MCHC, MCH, MCV, hematocrit, hemoglobin, and RBC counts, alongside reduced WBC counts, indicating enhanced physiological resilience. Moreover, erythrocyte malformation severity declined progressively with increasing activated carbon dosage, while survival rates improved markedly, reaching 97.5% in P5. Compared to previous studies, the use of coconut husk-derived activated carbon provided superior performance in promoting fish welfare. These findings underscore the potential of this sustainable, low-cost filtration material to enhance the ecological and economic viability of intensive and large-scale RAS operations. However, as a limitation, the study was conducted under short-term conditions in a controlled laboratory setup. Future investigations should focus on long-term field-scale trials, regeneration efficiency of the activated carbon, and cost-benefit analysis to fully assess its practicality and sustainability in commercial aquaculture. The development of circular waste-based filtration solutions such as this represents a promising step toward environmentally responsible aquaculture intensification.

Acknowledgment

This work was supported by the Penelitian Lektor (PL) scheme form Universitas Syiah Kuala Indonesia under Grant number 362/UN11.2.1/PG.01.03/SPK/PTNBH/2024.

References

Ahmed I, Reshi QM and Fazio F. 2020. The influence of the endogenous and exogenous factors on hematological parameters in different fish species: a review. *Aquac. Int.*, **28(3):** 869–899.

Ajien A, Idris JM, Md Sofwan N, Husen R and Seli H. 2022. Coconut shell and husk biochar: A review of production and activation technology, economic, financial aspect and application. *Waste Manag. Res.*, **41(1):** 37–51.

Akbar SA, Fatmawati DR, Dewi CD, Ismarica I, Nuzlia C, Nazlia S, Jalil Z, Iqbal TH, Hasan M and Lahori AH. 2025a. Toxicodynamic effects of chronic Pb^{2+} exposure on milkfish (*Chanos chanos*) and the phytoremediation role of *Caulerpa taxifolia*: Water quality, bioaccumulation, and multi-level biological responses. *Environ. Chem. Ecotoxicol*., **7:** 2319–2333.

Akbar SA, Hasan M, Jalil Z, Zulfahmi I, Iqhrammullah M and Safina N. 2025b. Enhanced ammonia nitrogen filtration using NaOH-activated Manihot utilissima peel carbon: Application in recirculating aquaculture systems for Nile tilapia. *Chemosphere*, **385:** 144537

Akbar SA, Mauliza L and Fazli RR. 2025c. Recent advances in carbon-based adsorbent materials for ammonium removal from water. *BIO Web of Conferences*, **156:** 02014.

Akbar SA, Nuzlia C, Hasan M, Jalil Z and Zulfahmi I. 2025d. Optimizing ammonia removal in recirculating aquaculture systems using NaOH-activated sugarcane bagasse carbon. *Sci. Technol. Asia*, **30(2):** 227–240.

Angellinnov F, Subhan A, Rengga WDP, Jumari A and Syahrial AZ. 2025. Effect of rice husk derived activated carbon surface coating on NMC 811 characteristics and performance as lithium-ion battery cathode. *Results Surf. Interfaces*, **19:** 100567.

Armstrong PR, Morchesky ZJ, Hess DT, Adu KW, Essumang DK, Tufour JK, Koranteng-Addo JE, Opoku-Boadu K and Mensah SY. 2014. Production of high surface area activated carbon from coconut husk. *MRS Online Proc. Libr.*, **1644(1):** 801.

Bardhan A, Abraham TJ, Das R and Patil PK. 2024. Visualization of poikilocytosis as an emerging erythrocytic biomarker for fish health assessment. *Anim. Res. One Health*, **2(2):** 136–157.

Barragán-Longoria MF, Pérez-Viveros KJ, Cadena-Ramírez A, Castro-Rosas J, Villagómez-Ibarra JR, Hernandez-Perez J, Hinojosa-Alvarez S, Gómez-Aldapa CA and Chavez-Santoscoy RA. 2025. Mesquite seed flour as a nutrient-rich alternative to fishmeal for common carp fingerlings (*Cyprinus carpio*): environmental, growth performance, transcriptomic and intestinal microbiota responses. *Aquac. Rep.*, **42:** 102768.

Chen H and Luo D. 2023. Application of haematology parameters for health management in fish farms. *Rev. Aquac.*, **15(2):** 704–737.

Dawood MAO, Alkafafy M and Sewilam H. 2022. The antioxidant responses of gills, intestines and livers and blood immunity of common carp (*Cyprinus carpio*) exposed to salinity and temperature stressors. *Fish Physiol. Biochem.*, **48(2):** 397–408.

Fatmawati A, Nurtono T and Widjaja A. 2023. Thermogravimetric kinetic-based computation of raw and pretreated coconut husk powder lignocellulosic composition. *Bioresour. Technol. Rep.*, **22:** 101500.

Fu J, Zhang J, Jin C, Wang Z, Wang T, Cheng X and Ma C. 2020. Effects of temperature, oxygen and steam on pore structure characteristics of coconut husk activated carbon powders prepared by one-step rapid pyrolysis activation process. *Bioresour. Technol.*, **310:** 123413.

Haider R, Sagadevan S, Al-Adaileh N, Fatimah I, Paiman S, Le MV and Johan MR. 2025. Sustainable activated carbon derived from coconut shell and betel nuts for energy storage and environmental remediation. *Diam. Relat. Mater.*, **154:** 112243.

Hamid M, Humaidi S, Saragi IR, Simanjuntak C, Isnaeni I, Azizah and Wijoyo H. 2024. The effectiveness of activated carbon from nutmeg shell in reducing ammonia (NH3) levels in fish pond water. *Carbon Trends*, **14:** 100324.

Hamid M, Nasution TI, Elfinita R, Wijoyo H and Isnaeni I. 2024. Reducing ammonia (NH3) levels in fish cage water using activated carbon adsorbent derived from purple corn cob. *Sci. Technol. Indones.*, **9(3):** 669–681.

Han B, Butterly C, Zhang W, He J and Chen D. 2021. Adsorbent materials for ammonium and ammonia removal: a review. *J. Clean. Prod.*, **283:** 124611.

Hoque F and Das A. 2025. Hematological techniques for diagnosis of fish diseases. In: Das BK and Kumar V (Eds.). *Lab. Tech. Fish Dis. Diagn.* Springer Nature Singapore.

Huno SKM, Das J, van Hullebusch ED, Annachhatre AP and Rene ER. 2023. Nitrate removal from groundwater using chemically modified coconut husk based granular activated carbon: characterization of the adsorbent, kinetics and mechanism. *Syst. Microbiol. Biomanuf.*, **3(2):** 370–383.

Jain A, Soni S and Verma KK. 2021. Combined liquid phase microextraction and fiber-optics-based cuvetteless micro-spectrophotometry for sensitive determination of ammonia in water and food samples by the indophenol reaction. *Food Chem.*, **340:** 128156.

Karatas T, Sokmen TO and Gur STA. 2025. Effects of pumpkin seed extract on growth, blood biochemistry, antioxidant status, immunity, and digestive enzymes of common carp (*Cyprinus carpio*) fingerlings. *Aquac. Rep.*, **43:** 102890.

Kasmuri N, Dzulkifli NFM, Ismail NA, Zaini N and Yaacob Z. 2022. An investigation of a mixture of coconut husk and rice husk as activated carbon for treatment of wastewater. *IOP Conf. Ser. Earth Environ. Sci.*, **1019(1):** 012048.

Khatun MM, Mostakim GM, Moniruzzaman M, Rahman UO and Islam MS. 2021. Distortion of micronuclei and other peripheral erythrocytes caused by fenitrothion and their recovery assemblage in zebrafish. *Toxicol. Rep.*, **8:** 415–421.

Kim B, Jin G, Byeon Y, Park SY, Song H, Lee C, Lee J, Noh J and Khim JS. 2025. Monitoring of the physiological responses of marine fishes to construction and operation noise from offshore wind farms. *Mar. Pollut. Bull.*, **218:** 118139.

Koner D, Banerjee B, Kumari A, Lanong AS, Snaitang R and Saha N. 2021a. Molecular characterization of superoxide dismutase and catalase genes, and the induction of antioxidant genes under the zinc oxide nanoparticle-induced oxidative stress in air-breathing magur catfish (*Clarias magur*). *Fish Physiol. Biochem.*, **47(6):** 1909–1932.

Koner D, Banerjee B, Kumari A, Lanong AS, Snaitang R and Saha N. 2021b. Molecular characterization of superoxide dismutase and catalase genes, and the induction of antioxidant genes under the zinc oxide nanoparticle-induced oxidative stress in air-breathing magur catfish (*Clarias magur*). *Fish Physiol. Biochem.*, **47(6):** 1909–1932.

Kumar N, Singh DK, Chandan NK, Thorat ST, Patole PB, Gite A and Reddy KS. 2023. Nano zinc enhances gene regulation of non specific immunity and antioxidative status to mitigate multiple stresses in fish. *Sci. Rep.*, **13(1):** 5015.

Liu C, Qiu T and Chen Y. 2023. Metal ion/metal hydroxide loaded resin for ammonia removal from solutions containing high salinity by ligand exchange: stability of metal ions during decomplexation of ammonia ligand. *Arab. J. Chem.*, **16(8):** 104879.

Mohamed AAR, El-Houseiny W, EL-Murr AE, Ebraheim LLM, Ahmed AI and El-Hakim YMA. 2020. Effect of hexavalent chromium exposure on the liver and kidney tissues related to the expression of CYP450 and GST genes of *Oreochromis niloticus* fish: role of curcumin supplemented diet. *Ecotoxicol. Environ. Saf.*, **188:** 109890.

Nguyen-tiêt AM, Letelier-Gordo CO and Aalto SL. 2025. Rapid H2S production in layers of freshwater and marine fish organic waste from recirculating aquaculture systems. *Aquac. Eng.*, **111:** 102578.

Pei X, Chu M, Tang P, Zhang H, Zhang X, Zheng X, Li J, Mei J, Wang T and Yin S. 2021. Effects of acute hypoxia and reoxygenation on oxygen sensors, respiratory metabolism, oxidative stress, and apoptosis in hybrid yellow catfish “Huangyou-1.” *Fish Physiol. Biochem.*, **47(5):** 1429–1448.

Prastiawan A, Jubaedah D and Syaifudin M. 2019. Pemanfaatan Karbon Aktif Kulit Pisang Kepok (*Musa Acuminate* L.) Pada Sistem Filtrasi Budidaya Ikan Nila (*Oreochormis Niloticus*). *Jurnal Akuakultru Rawa Indonesia*, **7(1):** 55-66.

Qin H, Long Z, Huang Z, Ma J, Kong L, Lin Y, Lin H, Zhou S and Li Z. 2023. A comparison of the physiological responses to heat stress of two sizes of juvenile spotted seabass (*Lateolabrax maculatus*). *Fishes*, **8(7):**.

Rehan K, Malaibari Z, Atieh M, Hussain I and Abu-Saud B. 2024. A highly efficient modified nano-activated carbon adsorbent for separation of ammonia from water: experimental and kinetics elucidations. *Chemosphere*, **364:** 143048.

Salaenoi J, Jurejan N, Yokthongwattana C, Pluempanupat W and Boonprab K. 2024. Characteristics of coconut husk cellulose and its effectiveness as a potassium permanganate absorbent for fishery applications. *Case Stud. Chem. Environ. Eng.*, **10:** 100975.

Tomy M, Geethamma GS, Aravind AM, Reshmi SS and Suryabai XT. 2024. Effect of activation environment on coconut-husk-derived porous activated carbon for renewable energy storage applications. *ACS Sustain. Resour. Manag.*, **1(7):** 1534–1547.

Wang Y, Deng M, Zhou S, Li L and Song K. 2024. Increasing fish production in recirculating aquaculture system by integrating a biofloc-worm reactor for protein recovery. *Water Res. X*, **24:** 100246.

Wijaya C, Sangadji NL, Muharja M, Widjaja T, Riadi L and Widjaja A. 2025. An integrated green fractionation of coconut husk: hydrothermal and deep eutectic solvent pretreatment for enhanced sugar and lignin production. *Bioresour. Technol. Rep.*, **29:** 102078.

Witeska M, Kondera E and Bojarski B. 2023. Hematological and hematopoietic analysis in fish toxicology—a review. *Animals*, **13(16):**.

Wu G, Liu HB, Ma C, Xu HM, Ren XZ and Sun W. 2025. Developments and application of fish school swimming model in recirculating aquaculture systems. *Ocean Eng.*, **319:** 120196.

Xu J, Lan M, Luo Y and Wu Y. 2024. Carbon, nitrogen, and phosphorus release characteristics and underlying mechanisms in fish manure from recirculating aquaculture systems under alternating aerobic-anaerobic conditions. *J. Environ. Chem. Eng.*, **12(6):** 114185.

Xu XN, Chen SL, Jiang ZX, Nissa M and Zou SM. 2022. Gill remodeling increases the respiratory surface area of grass carp (*Ctenopharyngodon idella*) under hypoxic stress. *Comp. Biochem. Physiol. A Mol. Integr. Physiol.*, **272:** 111278.

Xu Z, Cao J, Qin X, Qiu W, Mei J and Xie J. 2021. Toxic effects on bioaccumulation, hematological parameters, oxidative stress, immune responses and tissue structure in fish exposed to ammonia nitrogen: a review. *Animals*, **11(11):**.

Yang F, Zhang K, Lin Q, Pan H and Chen Z. 2025. Preparation of ultra-microporous oxygen-enriched carbon from activating waste sawdust with potassium formate for selective adsorption of CO2/CH4. *Sep. Purif. Technol.*, **372:** 133505.

Yuliusman, Sipangkar SP, Fatkhurrahman M, Farouq FA and Putri SA. 2020. Utilization of coconut husk waste in the preparation of activated carbon by using chemical activators of KOH and NaOH. *AIP Conf. Proc.*, **2255(1):** 060026.

Zhang T, Zhang L, Yin T, You J, Liu R, Huang Q, Shi L, Wang L, Liao T, Wang W and Ma H. 2023. Recent understanding of stress response on muscle quality of fish: from the perspective of industrial chain. *Trends Food Sci. Technol.*, **140:** 104145.

Zhao H, Peng K, Wang G, Mo W, Huang Y and Cao J. 2021. Metabolic changes, antioxidant status, immune response and resistance to ammonia stress in juvenile yellow catfish (*Pelteobagrus fulvidraco*) fed diet supplemented with sodium butyrate. *Aquaculture*, **536:** 736441.

Zhong A and Yan X. 2025. Erythropoiesis in teleost fishes: the fantastic biological process. *Rev. Aquac.*, **17(1):** e12960.

Zhou T, Zhai T, Ma J, Wu F and Zhang G. 2024. Sodium chloride-activated polymeric ferric sulfate-modified natural zeolite (Z-Na-Fe): application of bio-slow filtration for the removal of ammonia and phosphorus from micro-polluted cellar water. *J. Water Process Eng.*, **61:** 105367.